Broadband Filtering Magnetoelectronic Dipole Antenna with Quasi-Elliptic Gain Response

Wei, Zhaohui; Zhou, Zhao; Ren, Jian; Yin, Yingzeng

Published in:
I E E E Transactions on Antennas and Propagation

Publication date:
2020

Document Version
Accepted author manuscript, peer reviewed version

Broadband Filtering Magnetoelectronic Dipole Antenna with Quasi-Elliptic Gain Response

Zhaohui Wei, Zhao Zhou, Zhaoyang Tang, Jia Yuan Yin, Jian Ren *Member, IEEE,* and Yingzeng Yin

***Abstract*—A filtering magnetoelectronic dipole antenna (MEDA) with quasi-elliptic gain response and wide operating band is investigated. Different from the conventional MEDA, the antenna studied here is fed by fork-shaped microstrip line aperture-coupled excitation. The intrinsic radiation null of the MEDA at the lower passband edge is utilized, and a mathematical model is firstly put forward to demonstrate its working mechanism. Four driven stubs connected to the shorted walls of MEDA are used to excite the planar dipole arms. The parasitic inductor and the coupling capacitor introduced by driven stubs form an equivalent low-pass filter network, leading to a radiation null at higher frequency. Furthermore, a third radiation null is generated by introducing two quarter-wavelength U-shaped shorted stubs to improve the out-of-band suppression. Besides, due to the introduction of multiple coupling structure, including the fork-shaped microstrip line coupling slot and driven stubs, a wide operating band can be realized while maintains a low profile of 0.15 wavelength. Experimental results show that an impedance bandwidth of 53.5% (2.95 to 5.1 GHz) is achieved and an out-of-band suppression level higher than 17.9 dB is obtained. What's more, an average gain of 8 dBi and good radiation patterns are realized over the whole operating band.**

***Index Terms*—broadband antenna; filtering antenna; magnetoelectronic dipole antenna (MEDA); quasi-elliptic gain response.**

I. Introduction

Past three decades have witnessed the significant development of modern wireless communication. As a limited resource, the spectrum is getting more and more crowded, which may lead to serious interference between adjacent frequency bands. To address this issue, filtering antennas are widely studied due to their advantages of improved in-band selectivity, enhanced out-of-band suppression, and integrated filtering performance [1, 2]. To realize a filtering antenna, various approaches have been investigated. A common method is to integrate a bandpass filter and an antenna radiator into a single module [3–9]. Although a good filtering characteristic can be obtained, the multi-stage resonators used in this method may introduce insertion loss and degrade gain performance. To address this issue, filtering antennas without extra filtering circuits have been widely studied [10–19]. In [10–15], filtering responses were realized by introducing resonant structures into feeding networks or antenna radiators, making energy captured by the resonant structures and not effectively radiated in band of interest. Different resonant structures have been designed, such as $\lambda/2$ open-circuited lines [10, 11], $\lambda/4$ short-circuited lines [12, 13], and slots [14, 15]. Apart from using resonant structures, cross coupling theory is also applied to design filtering antennas. Many methods are used to create the cross-coupling path in [16–17]. As proposed in [17], by introducing two additional probes, two cross-coupling paths were built up, which generated two radiation nulls at both passband edges.

Manuscript received XXXX. This work was supported in part by the National Natural Science Foundation of China under Grant No. 61801354. (Corresponding author: Jian Ren and Yingzeng Yin.)

Z. Wei, Z. Zhou, Z, Tang, J. Ren and Y. Yin are with the National Key Laboratory of Antennas and Microwave Technology, Xidian University, Xi'an, Shaanxi, 710071, China. (email: Jian Ren: renjian@xidian.edu.cn, Yingzeng Yin: yyzeng@mail.xidian.edu.cn).

Y. J. Yin is with the School of Physics and Optoelectronic Engineering, Xidian University, Xi'an, Shaanxi, 710071, China.

Color versions of one or more of the figures in this communication are available online at http://ieeexplore.ieee.org.

Digital Object Identifier xxxxxxxxxx

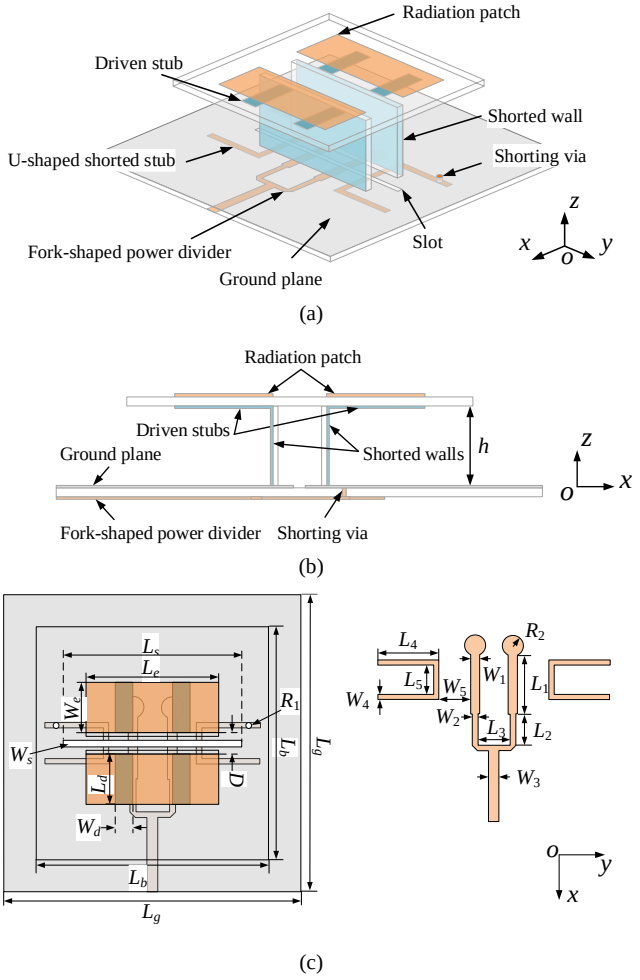

Fig. 1. Geometry of the proposed filtering antenna. (a) 3D view. (b) Side view. (c) Top view (left) and feeding structure (right). (Parameters: L_s = 39, L_e = 33, L_d = 15, L_b = 55, L_g = 150, L_1 = 19, L_2= 11, L_3 = 10, L_4 = 12, L_5 = 3, W_1 = 2.5, W_2= 1.7, W_3 = 2.7, W_4 = 1.5, W_5 = 3, W_s = 0.7, W_d = 5, W_e = 15, D = 4, R_1 = 0.7, R_2 = 3, h = 10.5, h_1 = 1.5, h_2 = 1. Unit: mm)

The principle of null-generation methods above is that the energy cannot be transmitted to antenna radiator. Different from these designs, filtering antennas are also achieved based on radiation cancellation principle [19–22]. In [19, 20], the currents on the radiation patch and the parasitic patch were same in amplitude but opposite in phase, leading to a radiation cancellation in far field. In [21], the currents on the driven stubs became disordered due to the introduction of three shorting pins, which generated a radiation null at the lower passband edge. The authors in [22] introduced a strip and three posts into a dielectric resonator antenna (DRA) to compose a dual-loop structure. Owing to the radiation cancellation of opposite currents of the dual-loop, the filtering performance was obtained.

Magnetoelectronic dipole antenna (MEDA), since firstly proposed by Luk *et al.* [23, 24], has attracted much attention due to its advantages of wide operation band, stable antenna gain, low back

radiation and symmetric E- and H-plane radiation patterns. In the past few years, extensive studies on MEDA have been carried out, including wideband MEDA [25–26], circular polarized MEDA [27], reconfigurable MEDA [28], mm-wave MEDA [29] and so on. Till now, main studies focus on the radiation performance within the operating band, while the out-of-band characteristic has not been paid much attention. In [30], the magnetoelectronic dipole filtering antenna was studied by introducing slot structures to the conventional MEDA, in which the intrinsic radiation null at the lower stopband was also utilized. In [32], the filtering frequency response was realized by symmetrically inserting four slots on the patches and elaborately design the feeding lines. Besides, by using a feeding network with a hook-shaped self-coupled line [33], a radiation null at the upper band edge and a high out-of-band radiation suppression were obtained.

In this paper, a broadband magnetoelectronic dipole filtering antenna with quasi-elliptic gain response is investigated. Inspired by the design in [25], the antenna is fed by fork-shaped microstrip line aperture-coupled excitation and the radiation patches are excited by four driven stubs via coupling. Three radiation nulls can be obtained at the passband edges based on different principles. The intrinsic radiation null of the MEDA at the lower passband edge is utilized, which can significantly reduce the complexity of filtering antenna. An equivalent mathematical model is built up and analyzed to better understand the principle of the intrinsic radiation null's generation. In addition, four driven stubs are introduced to obtain a radiation null at the upper passband edge. Moreover, to further improve the out-of-band radiation suppression level at the lower stopband, two quarter-wavelength U-shaped short-circuited stubs are employed to obtain the third radiation null. By introducing the multiple coupling structure including the fork-shaped microstrip line coupling slot and driven stubs, a good impedance can be obtained while maintains a low profile. Measured results show that a wide impedance bandwidth from 2.95 to 5.1 GHz for VSWR < 1.5 is realized. An average gain of 8 dBi and good radiation patterns are obtained across the whole operating band. What's more, enhanced roll-off rates at the passband edges and a high out-of-band suppression level better than 17.9 dB are achieved. To validate the synthesis and design, the proposed filtering antenna is fabricated and tested. The measured results are in good accordance with the simulated ones.

II. Antenna Configuration and Design

A. Configuration

Figure 1 depicts the configuration of the proposed wideband filtering antenna. It mainly consists of radiation patches, driven stubs, shorted walls, a feeding network and a ground plane. The radiation patches ($L_e \times W_e$) are printed on the top layer of a substrate with a thickness of h_1. Four symmetrical driven stubs are printed on the bottom surface of the substrate and each stub has a size of $L_d \times W_d$. The shorted walls with a height of h are vertically oriented underneath the substrate, which are directly connected to the driven stubs. The shorted walls are printed on two 0.5-mm-thick substrates and the separation between them is D. The feeding network and the ground plane are etched on a square printed circuit board with a thickness of h_2 and a length of L_g. The metal printed on the top surface of the substrate acts as the ground plane of the antenna. A slot with a width W_s and a length L_s is located at the center position of the ground plane. The bottom layer of square substrate is the fork-shaped microstrip power divider, whose two microstrip branches are extended perpendicularly cross the slot on the top surface. To provide a better impedance matching, its two output ports are terminated by two circular-shaped patches with a radius of R_2. Besides, two identical U-shaped shorted stubs are introduced, as depicted in Fig. 1(c). All substrates are fabricated with F4B with relative permittivity of 2.65 and loss tangent of 0.002.

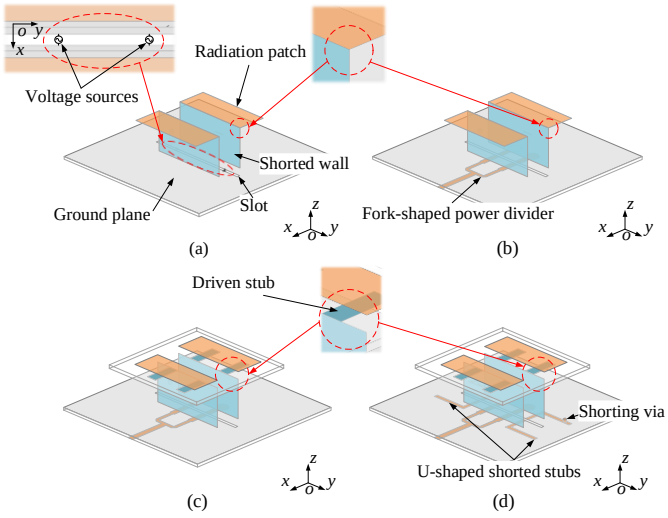

Fig. 2. Evolution of the proposed filtering antenna. (a) Antenna-A. (b) Antenna-B. (c) Antenna-C. (d) Pro. Antenna.

B. Evolution

To better present the design process, three reference antennas, denoted as Antenna-A, Antenna-B, and Antenna-C, are shown in Fig. 2 to compare with the proposed filtering antenna (Pro. antenna). As shown in Fig. 2(a), Antenna-A is a typical slot-fed magnetoelectronic dipole antenna with two identical voltage sources. The simulated VSWR and realized gain of Antenna-A are depicted in Fig. 3(a). With reference to the figure, it can be seen that a radiation null occurs at the lower passband edge, marked as Null 1, while a flat gain of 8 dBi is realized in its operating frequency band. A radiation suppression level of 13 dB is realized at the lower stopband. However, at the higher stopband, the VSWR slowly deteriorates and the corresponding gain slightly decreases with frequency increasing, indicating no filtering performance.

For physical realization, the two ideal voltage sources in Antenna-A are substituted by a fork-shaped power divider in Antenna-B as slot-coupled excitation. To improve the matching, the power divider has its two microstrip branches attached with two circular discs at the ends. The simulated VSWR and realized gain of Antenna-B are also exhibited in Fig. 3(a). Comparing to Antenna-A, an upsurge of VSWR occurs at the higher stopband of Antenna-B and the realized gain of the Antenna-B obviously decreases.

To improve the suppression level at higher stopband, the direct connection between the radiation patches and shorted walls is replaced by capacitive coupling, which is realized with two pairs of driven stubs connected to shorted walls. The new antenna is referred as Antenna-C, as illustrated in Fig. 2(c). As can be seen from the figure, the driven stubs are horizontally arranged beneath the radiation patches. Figure 3(b) shows the simulated VSWR and realized gain of Antenna-C. Comparing to Antenna-B, it is clearly found that a new radiation null (Null 2) is generated at the higher passband edge and a high suppression level as high as 22 dB at the higher stopband is obtained. Besides, the impedance bandwidth is also distinctly enhanced. Despite two radiation nulls are obtained, the filtering response of the antenna can be further enhanced. Two U-shaped shorted stubs are introduced into the antenna-C, obtaining the proposed antenna, as depicted in Fig. 2(d). a comparison of the simulated VSWRs and realized gains

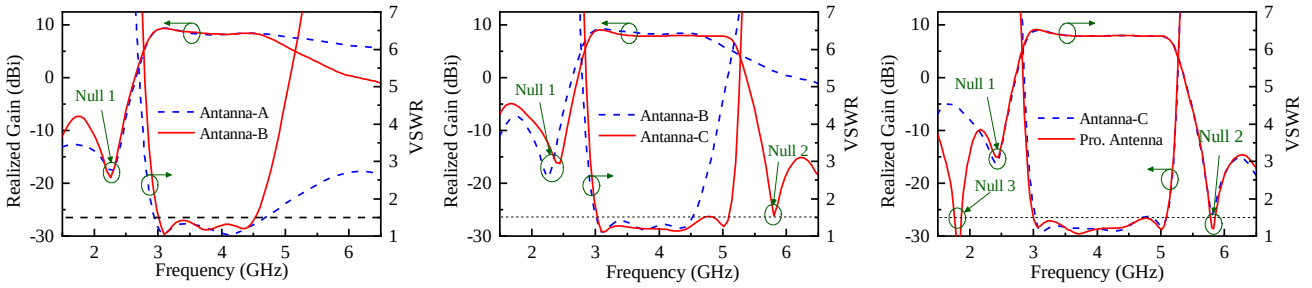

Fig. 3. VSWRs and realized gains comparisons. (a) Between Antenna-A and -B. (b) Between Antenna-B and -C. (c) Between Antenna-C and Pro. Antenna.

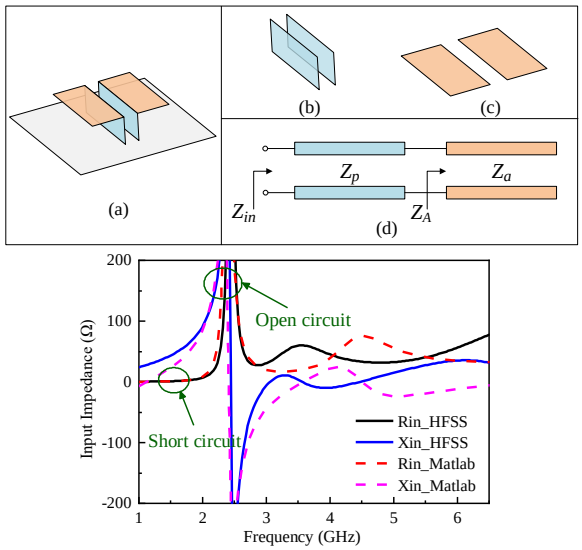

Fig.4. (a) A magnetoelectronic dipole antenna. (b) A parallel-plate transmission line. (c) A planar dipole. (d) A mathematic model. (e) Simulated and calculated input impedances of the antenna.

between antenna-C and Pro. antenna is given in Fig. 3(c). a third radiation null (Null 3) can be observed. an out-of-band radiation suppression level better than 18 dB is obtained at the lower stopband. By far, the final structure of the proposed filtering antenna is determined and a good filtering performance with three radiation nulls is realized.

III. Working Principle

A. *Analysis of Null 1*

To illustrate the principle of Null 1 at 2.44 GHz, an approximate mathematical model based on the transmission line model is proposed. To reveal the intrinsic characteristic of MEDA, no specific feeding structure is included. The structure of MEDA and its equivalent model are depicted in Fig. 4. As shown in Fig. 4, the antenna can be divided into a planar electric dipole and shorted walls. To determine the input impedance of MEDA, the modeling process involves the following three steps. The first step is to consider the dipole as a lossy transmission line [34], and its input impedance can be obtained as follows:

$$Z_A = Z_a \frac{\sinh 2\alpha l - \frac{\alpha}{\beta}\sin 2\beta l}{\cosh 2\alpha l - \cos 2\beta l} - jZ_a \frac{\frac{\alpha}{\beta}\sinh 2\alpha l + \sin 2\beta l}{\cosh 2\alpha l - \cos 2\beta l} \quad (1)$$

In this expression, $Z_a = 120[\ln(2l/a) - 1]$, is the average characteristic impedance of the dipole, where l is the length of the dipole, a is the effective width of the dipole, $\alpha = R/(2 \times Z_a)$, is the effective decay constant of the dipole, where R is the radiation resistance [34], $\beta =$

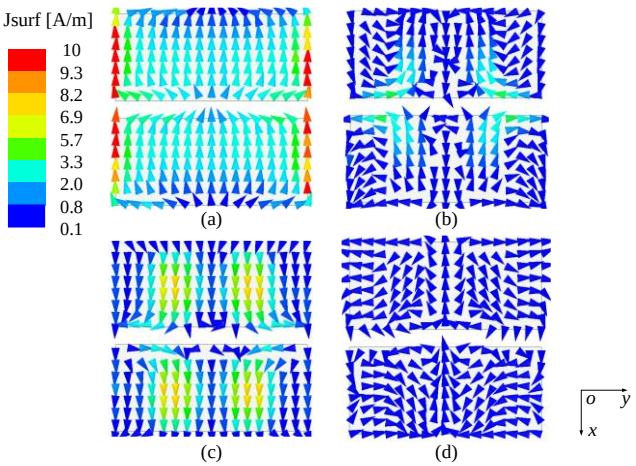

Fig. 5. Current vector distribution of the proposed antenna. (a) At passband (4 GHz) (b) At Null 1 (2.44 GHz). (c) At Null 2 (5.8 GHz). (d) At Null 3 (1.84 GHz).

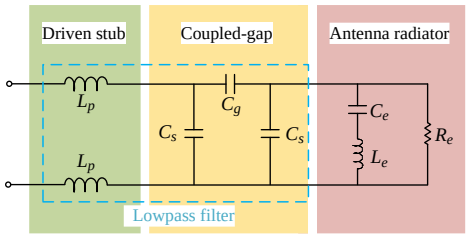

Fig. 6. Equivalent circuit of the proposed antenna.

$2\pi/\lambda_{es}$, is the phase constant of the dipole, where $\lambda_{es} = \lambda_0/\sqrt{\varepsilon_{es}}$ and ε_{es} is the effective dielectric constant of the dipole.

The second step is to model the shorted walls as a parallel-plate transmission line, and its characteristic impedance is

$$Z_p = \frac{\eta d}{W} \quad (2)$$

where $\eta = 120\pi\ \Omega$ is the wave impedance of free space, d and W denote the spacing and width of the parallel-plate transmission line, respectively.

The third step is to transform the input impedance of the dipole along the parallel-plate transmission line. By using the impedance transformation formula [35], the input impedance of a lossless transmission line terminated by an arbitrary load Z_L can be obtained:

$$Z_{in} = Z_0 \frac{Z_L + jZ_0 \tan(\beta l)}{Z_0 + jZ_L \tan(\beta l)} \quad (3)$$

Putting (1) and (2) substitute into (3), the input impedance of MEDA is obtained. Figure 4(e) shows the simulated input impedances obtained with full-wave simulation and theatrically calculation. As shown in Fig. 4(e), the input resistance becomes extremely high while the input reactance equals to zero at around 2.44 GHz, which indicates

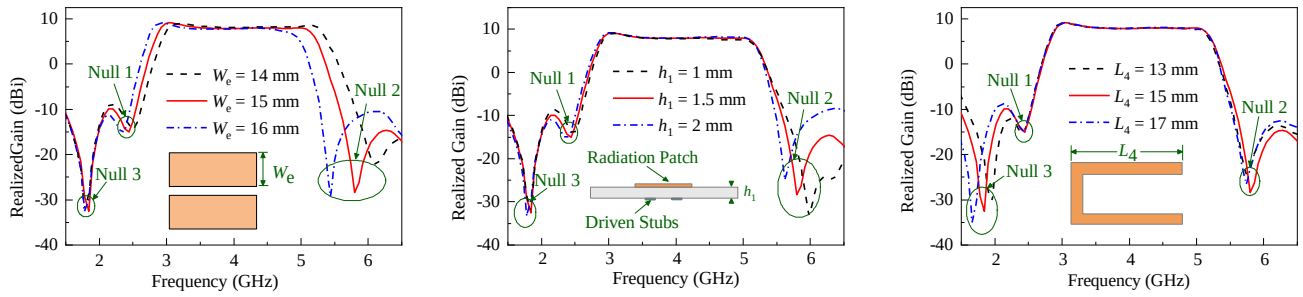

(a) (b) (c)

Fig. 7. Simulated realized gains of the proposed antenna (a) with different W_e. (b) with different h_1. (c) with different L_4.

a parallel resonance occurs. In this case, the antenna is equivalent to open circuit condition, leading to the serious impedance mismatching. Nearly all the energy in the feeding network is fully reflected back and no energy is radiated by antenna, resulting in Null 1. The current distribution at 2.44 GHz is depicted in Fig. 5(b). As observed, comparing to the current distribution at passband, the current on radiation patch is fairly weak, indicating little energy can be transmitted to the radiation patch. It confirms the validity of the theory.

B. *Analysis of Null 2*

To explain the principle of Null 2, an equivalent circuit model of the antenna is depicted in Fig. 6. For simplicity, only the equivalent circuit for driven stubs and radiation patches is shown. The electric dipole is replaced by a series resonant circuit L_e C_e R_e. The driven stubs can be replaced by the series inductor L_d, whose value mainly depends on the length of the driven stubs. The narrow gap between the driven stubs and the radiation patches provides a capacitive coupling. It can be modeled as a π-type network with a series capacitor C_g and two identical parallel capacitors C_s, whose value is determined by the width of the coupled-gap.

The equivalent inductor and capacitor compose a one-order lowpass filter. Its cutoff frequency can be adjusted by modifying the length of the driven stubs and the height of the gap. In this design, the cut-off frequency is fixed at the frequency where Null 2 occurs. When operating at the passband, the driven stubs have no effect on the power transmission and energy can be smoothly transmitted to the radiation patches. While operating at the stopband, the energy would be cut off by the driven stubs and cannot be transmitted to the radiation patches, which leads to the radiation null at 5.8 GHz. The current distribution on the radiation patch is shown in Fig. 5(c). With reference to the figure, unlike the current distribution at passband, it mainly concentrates on the area over the driven stubs. Observing other area on the patch, the current is very weak, which gives a hint that energy resonates between the driven stubs and the patch and little energy can be radiated, leading to the radiation null at 5.8 GHz. Another point worthy mentioning is that the radiation null at upper passband edge can also be obtained by utilizing one or three pairs of driven stubs. This is because the equivalent circuit is similar. Since the proposed antenna is easier to obtain a good impedance match than that with one pair of stubs and is simpler in structure than that with three pairs of stubs, thus two pairs of driven stubs are finally selected.

C. *Analysis of Null 3*

To further improve the out-of-band radiation suppression level, two U-shaped shorted stubs are added at both sides of the slot. According to [35], a quarter-wavelength short-circuited stub is equivalent to a parallel resonator, and the relation between resonant frequency and total length can be expressed as:

$$f = \frac{c}{4l\sqrt{\varepsilon_r}} \tag{4}$$

where, f is the resonant frequency of the shorted stubs, c is the velocity of light in free space, ε_r is the effective dielectric constant of the substrate, and $l = 2L_4 + L_5$ is the total length of the shorted stubs. By appropriately tuning the total length l of the shorted stub, the resonant frequency can be shifted to a desired band. When it resonates, the power transmitted to antenna would be absorbed by the shorted stubs and dissipated in the form of heat. This makes the energy not transmitted to the antenna, thus generating radiation Null 3. Besides, another point worthy mentioning is that if two driven stubs with different lengths are utilized, two different radiation nulls would be obtained. For simplicity, two identical stubs are selected.

IV. Parameter Study

Some key parameters affecting the location of radiation nulls are analyzed. Figure 7(a) shows the effect of the parameter W_e on the realized gain. It can be seen that Null 1 and Null 2 simultaneously move toward the higher frequency band as W_e decreaes. This is because the current path length becomes shorter. We can also see that the location of Null 3 remains unchanged, which indicates that the length of dipole W_e has little effect on Null 3.

The effect of the parameter h_1 on the realized gain is displayed in Fig. 7(b). As observed in Fig. 7(b), Null 1 and Null 3 are nearly unchanged, while Null 2 moves toward lower frequency band as h_1 decreases. According to the above-mentioned analysis, the driven stubs and the coupled gap are composed of a lowpass filter. As the separation h_1 decreases, the value of the equivalent capacitor becomes larger while that of the equivalent inductor remains unchanged, the resonant frequency of the equivalent lowpass filter moves downwards. As a consequence, Null 2 moves toward lower frequency band.

The dimension (L_4) of the U-shaped shorted stubs is analyzed.As shown in Fig. 7(c), Null 3 shifts to lower frequency band as L_4 increases. This is mainly because the U-shaped shorted stub works as a series resonant circuit. As L_4 increases, the current path length becomes longer, thus Null 3 moves toward lower frequency band.

V. Antenna Implement

A. *Design Guideline*

Based on the above-mentioned analysis, a design guideline for the designed filtering antenna is summarized. The design procedure involves the following four steps:

1) Determine the sizes of the radiation patch ($L_e \times W_e$) according to the desired center frequency. The resonant frequency of the radiation patch is mainly controlled by its lengths L_e. Since the end effects at the two edges of the radiation patch would extend the resonant length, thus the initial length $L_e = 0.2\lambda_0$ (λ_0 is the wavelength corresponding to center frequency) is selected. For wideband operation, the initial width

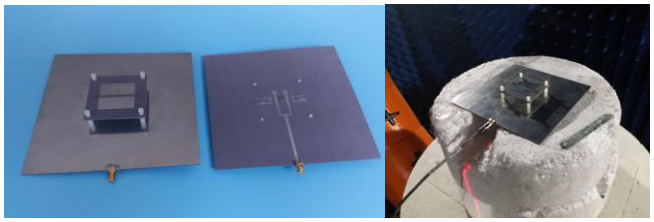

(a) (b)

Fig. 8 Photographs of the proposed antenna. (a) Prototype. (b) Measurement.

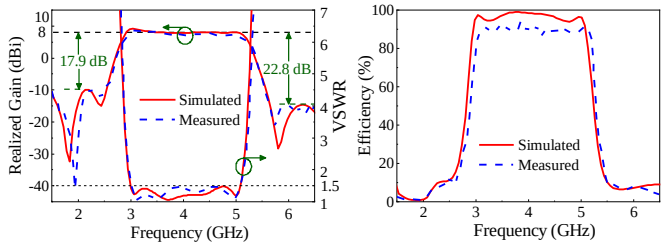

(a) (b)

Fig. 9 (a) Simulated and measured VSWRs and realized gains. (b) Simulated and measured efficiencies.

$W_e = 0.44\lambda_0$ is selected. Adjust the length L_e of the radiation patch to tune the intrinsic radiation null to the desired lower passband edge frequency.

2) Introduce driven stubs to the antenna to generate a radiation null at the higher passband edge. For ease of installation, the driven stubs can be printed on the bottom layer of the top substrate. The spacing $h_1$between the driven stubs and the radiation patch is an important parameter. By appropriately adjusting the spacing h_1, the radiation null can be shifted to the desired higher passband edge frequency.

3) Add two identical U-shaped stubs terminated with shorting pins to further improve the radiation suppression level at the lower stopband. Resonant frequency of the U-shaped stubs mainly depends on the length ($L_4 \times 2 + L_5$). Tune the length to adjust Null 3 to the desired frequency band, the out-of-band radiation would be effectively suppressed.

4) Finally, refine each parameter to optimize the design for a good filtering performance and a required bandwidth.

B. Experiment

A prototype of the proposed filtering antenna is fabricated and tested for validation. The photographs of the designed antenna are shown in Fig. 8. The voltage standing wave ratio (VSWR) is measured using a vector network analyzer AV3672B. A SATIMO near-field measurement system is used to measure the radiation characteristics of the antenna. The simulated and measured VSWRs and realized gains are illustrated in Fig. 9(a). Referring to the figure, it can be seen that the proposed antenna achieves a relative impedance bandwidth of 53.5% (2.95 to 5.1 GHz). And a flat realized gain around 8 dBi is obtained in the operating band. Besides, the gain response exhibits sharp roll-off rates at the desired stopband.

The simulated and measured radiation efficiency and patterns are shown in Fig. 9(b) and Fig. 10, respectively. With reference to the Fig. 9(b), it can be found that the measured radiation efficiency is about 90% in the passband while 10% in the stopband, which gives a hint that a high frequency selectivity is realized. Besides, the measured efficiency in passband is a little less than the simulated one, which may be caused by the loss of the feeding network, fabrication tolerance and effect of test surroundings. Referring to the Fig. 10, symmetrical radiation patterns can be observed both in E- and H-plane. A wide beamwidth and a low cross-polarization are obtained over the whole operating band.

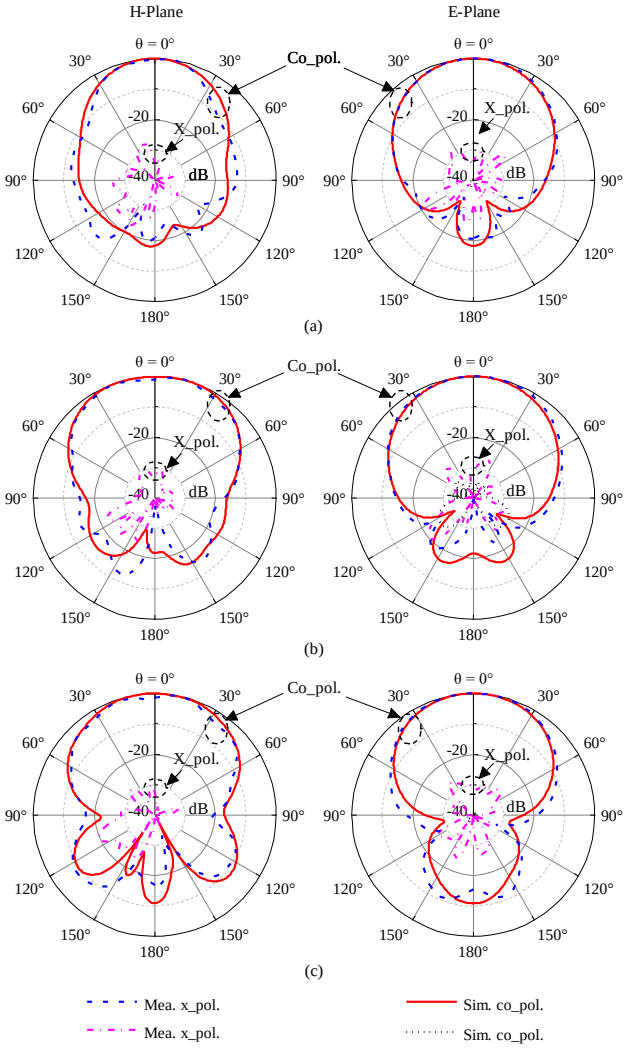

Fig. 10 Simulated and measured radiation patterns. (a) 3 GHz. (b) 4 GHz. (c) 5 GHz.

TABLE I
COMPARISON OF THE PROPOSED AND REFERENCE ANTENNAS

Ref.	Bandwidth	VSWR	Profile	Gain (dBi)	Out-of-band suppression (dB)
[1]	16.3%	< 2	/	2.41	/
[12]	46.1%	< 2	0.009 λ_g	5	13
[15]	20.3%	< 2	0.1 λ_g	9.05	25
[19]	8.3%	< 2	/	6.83	12
[30]	55.4%	< 1.5	0.22 λ_g	7.8	17
[31]	17.6%	< 2	0.04 λ_g	8	17
[32]	27.6%	< 1.5	0.10 λ_g	8.2	20
[33]	24.7%	< 2	0.20 λ_g	7.6	15
Pro.	53.5%	< 1.5	0.15 λ_g	8	17.9

Note: λ_g denotes the wavelength corresponding to the center frequency

C. Comparison

In this section, a comparison between other filtering antennas in the published literatures and the presented antenna here is shown in Table I. With reference to the table, the proposed filtering antenna achieves a wider bandwidth of 53.5% for VSWR < 1.5 than all the mentioned references except [30]. Comparing to [30], due to the introduction of multiple coupling structure including the fork-shaped microstrip line

coupling slot and driven stubs, a lower profile height can be obtained while maintains a wide impedance bandwidth. Meanwhile, the proposed filtering antenna also achieves a high gain, a high out-of-band radiation suppression level and stable radiation patterns.

VI. Conclusion

In this paper, a broadband magnetoelectronic filtering antenna with quasi-elliptic gain response is presented. By introducing the fork-shaped microstrip line aperture-coupled excitation and four driven stubs, two radiation nulls are obtained at the passband edges, exhibiting a good filtering performance. To understand the principle of the radiation nulls, a mathematical model and an equivalent circuit are proposed. In addition, to further improve the out-of-band radiation suppression level at the lower stopband, two quarter-wavelength U-shaped shorted stubs are employed to obtain the third radiation null. Parameter studies are provided to analyze the effect of various parameters. To validate the design, a prototype antenna operating at center frequency of 4 GHz is fabricated and measured. The simulated and measured results show a wide impedance bandwidth of 53.5% for VSWR < 1.5 (from 2.95 to 5.1 GHz) is realized. An average gain of 8 dBi and a stable radiation pattern are achieved within the whole operating band. What's more, an out-of-band suppression level better than 17.9 dB is achieved.

References

[1] W. J. Wu, Y. Z. Yin, S. L. Zuo, Z. Y. Zhang, and J. J. Xie, "A new compact filter-antenna for modern wireless communication systems," *IEEE Antennas Wireless Propag. Lett.*, vol. 10, pp. 1131–1134, 2011.

[2] C. X. Mao, S. Gao, Y. Wang, B. Sanz-Izquierdo, Z. Wang, F. Qin, Q. X. Chu, J. Li, G. Wei, and J. Xu, "Dual-band patch antenna with filtering performance and harmonic suppression," *IEEE Trans. Antennas Propag.*, vol. 64, no. 9, pp. 4074–4077, 2016.

[3] R. Lovato, and X. Gong, "A third-order SIW-integrated filter/antenna using two resonant cavities," *IEEE Antennas Wireless Propag. Lett.*, vol. 17, no. 3, pp. 505–508, Mar. 2018.

[4] K. Dhwaj, J. M. Kovitz, H. Tian, L. J. Jiang, and T. Itoh, "Half-mode cavity-based planar filtering antenna with controllable transmission zeroes," *IEEE Antennas Wireless Propag. Lett.*, vol. 17, no. 5, pp. 833–836, May. 2018.

[5] C. X. Mao, S. Gao, Y. Wang, Q. Luo, and Q. X. Chu, "A shared-aperture dual-band dual-polarized filtering-antenna-array with improved frequency response," *IEEE Trans. Antennas Propag.*, vol. 65, no. 4, pp. 1836–1844, Apr. 2017.

[6] H. Cheng, Y. Yusuf and X. Gong, "Vertically integrated three-pole filter/antennas for array applications," *IEEE Antennas Wireless Propag. Lett.*, vol. 10, pp. 278–281, 2011.

[7] C. X. Mao, S. Gao, Y. Wang, Q. Luo, and Q. X. Chu, "A shared-aperture dual-band dual-polarized filtering-antenna-array with improved frequency response," *IEEE Trans. Antennas Propag.*, vol. 65, no. 4, pp. 1836–1844, Apr. 2017.

[8] Q. Wu, X. Zhang and L. Zhu, "Co-design of a wideband circularly polarized filtering patch antenna with three minima in axial ratio response," *IEEE Trans. Antennas Propag.*, vol. 66, no. 10, pp. 5022–5030, Oct. 2018

[9] Z. H. Jiang and D. H. Werner, "A compact, wideband circularly polarized co-designed filtering antenna and its application for wearable devices with low sar," *IEEE Trans. Antennas Propag.*, vol. 63, no. 9, pp. 3808–3818, Sept. 2015.

[10] X. Y. Zhang, Y. Zhang, Y. M. Pan, and W. Duan, "Low-profile dual-band filtering patch antenna and its application to LTE MIMO system," *IEEE Trans. Antennas Propag.*, vol. 65, no 1, pp. 103–113, 2017.

[11] J. Deng, S. Hou, L. Zhao, and L. Guo, "Wideband-to-Narrowband tunable monopole antenna with integrated bandpass filters for uwb/wlan applications," *IEEE Antennas Wireless Propag. Lett.*, vol. 16, pp. 2734–2737, 2017.

[12] H. T. Hu, F. C. Chen, and Q. X. Chu. "Novel broadband filtering slotline antennas excited by multimode resonators," *IEEE Antennas Wireless Propag. Lett.*, vol. 16, pp. 489–492, 2017.

[13] P. F. Hu, Y. M. Pan, X. Y. Zhang and B. J. Hu, "A compact quasi-isotropic dielectric resonator antenna with filtering response," *IEEE Trans Antennas Propag.*, vol. 67, no. 2, pp. 1294–1299, Feb. 2019

[14] J. Y. Jin, S. Liao, Q. Xue, "Design of filtering-radiating patch antennas with tunable radiation nulls for high selectivity," *IEEE Trans. Antennas Propag.*, vol. 66, no. 4, pp. 2125–2130, 2018.

[15] P. F. Hu, Y. M. Pan, X. Y. Zhang, and S. Y. Zheng, "A compact filtering dielectric resonator antenna with wide bandwidth and high gain," *IEEE Trans. Antennas Propag.*, vol. 64, no. 8, pp. 3645–3651, Aug. 2016.

[16] B. Zhang, and Q. Xue, "Filtering antenna with high selectivity using multiple coupling paths from source/load to resonators," *IEEE Trans. Antennas Propag.*, vol. 66, no. 8, pp. 4320–4325, 2018.

[17] P. F. Hu, Y. M. Pan, X. Y. Zhang, and B. J. Hu, "A filtering patch antenna with reconfigurable frequency and bandwidth using F-shaped probe," *IEEE Trans. Antennas Propag.*, vol. 67, no. 1, pp. 121–130, Jan. 2019.

[18] P. F. Hu, Y. M. Pan, K. W. Leung, and X. Y. Zhang, "Wide-/dual-band omnidirectional filtering dielectric resonator antennas," *IEEE Trans. Antennas Propag.*, vol. 66, no. 5, pp. 2622–2627, May. 2018.

[19] J. F. Qian, F. C. Chen, Q. X. Chu, Q. Xue, and M. J. Lancaster, "A novel electric and magnetic gap-coupled broadband patch antenna with improved selectivity and its application in MIMO system," *IEEE Trans. Antennas Propag.*, vol. 66, no. 10, pp. 5625–5629, Oct. 2018.

[20] W. Duan, X. Y. Zhang, Y. M. Pan, J. X. Xu, and Q. Xue, "Dual-polarized filtering antenna with high selectivity and low cross polarization", *IEEE Trans. Antennas Propag.*, vol. 64, no. 10, pp. 4188–4196, Oct. 2016.

[21] X. Y. Zhang, W. Duan, and Y. M. Pan, "High-gain filtering patch antenna without extra circuit," *IEEE Trans. Antennas Propag.*, vol. 63, no. 12, pp. 5883–5888, 2015.

[22] Y. Liu, K. W. Leung, J. Ren, and Y. Sun, "Linearly and circularly polarized filtering dielectric resonator antennas," *IEEE Trans. Antennas Propag.*, to be published, 2019.

[23] K. -M. Luk, and H. Wong, "A new wideband unidirectional antenna element," *Int. J. Microw. Opt. Technol.*, vol. 1, no. 1, pp. 35–44, Jun. 2006.

[24] K. -M. Luk, and H. Wong, "Complementary wideband antenna," U. S. Patent 7843389, Nov. 30, 2010.

[25] X. Cui, F. Yang, M. Gao, L. Zhou, Z. Liang, and F. Yan, "A wideband magnetoelectric dipole antenna with microstrip line aperture-coupled excitation," *IEEE Trans. Antennas Propag.*, vol. 65, no. 12, pp. 7350–7354, Dec. 2017.

[26] L. Ge, and K. -M. Luk, "A magneto-electric dipole for unidirectional UWB communications," *IEEE Trans. Antennas Propag.*, vol. 61, no. 11, pp. 5762–5765, Nov. 2013.

[27] L. Ge, M. Li, Y. Li, H. Wong, and K. -M. Luk, "Linearly polarized and circularly polarized wideband dipole antennas with reconfigurable beam direction," *IEEE Trans. Antennas Propag.*, vol. 66, no. 4, pp. 1747–1755, Apr. 2018.

[28] F. Wu, and K. -M. Luk, "Wideband tri-polarization reconfigurable magneto-electric dipole antenna," *IEEE Trans. Antennas Propag.*, vol. 65, no. 4, pp. 1633–1641, Apr. 2017.

[29] Y. Li, and K. -M. Luk, "A multibeam end-fire magnetoelectric dipole antenna array for millimeter-wave applications," *IEEE Trans. Antennas Propag.*, vol. 64, no. 7, pp. 2894–2904, Jul. 2016.

[30] G. Zhang, L. Ge, J. Wang, and J. Yang, "Design of a 3-D integrated wideband filtering magneto-electric dipole antenna," *IEEE Access*, vol. 7, pp. 4735–4740, 2018.

[31] W. Yang, S. Chen, Q. Xue, W. Che, G. Shen, and W. Feng, "Novel filtering method based on metasurface antenna and its application for wideband high-gain filtering antenna with low profile," *IEEE Trans. Antennas Propag.*, vol. 67, no. 3, pp. 1535–1544, Mar. 2019.

[32] S. J. Yang, Y. M. Pan, Y. Zhang, Y. Gao and X. Y. Zhang, "Low-profile dual-polarized filtering magneto-electric dipole antenna for 5G applications," *IEEE Trans. Antennas Propag. (Early Access).*

[33] Y. Zhang, X. Y. Zhang, L. Gao, Y. Gao and Q. H. Liu, "A two-port microwave component with dual-polarized filtering antenna and single-band bandpass filter operations," *IEEE Trans. Antennas Propag. (Early Access*).

[34] C. A. Balanis, *Antenna Theory: Analysis and Design*. John Wiley, 3rd ed., New York, NY, USA: John Wiley & Sons, 2005.

[35] D. M. Pozar, *Microwave engineering.* Boston, MA, USA: Artech House, 1998.